

## Gels

## Amino Acid Chirality and Ferrocene Conformation Guided Self-Assembly and Gelation of Ferrocene–Peptide Conjugates

Bimalendu Adhikari,<sup>\*,[a]</sup> Charanpreet Singh,<sup>[a]</sup> Afzal Shah,<sup>[a, c]</sup> Alan J. Lough,<sup>[b]</sup> and Heinz-Bernhard Kraatz<sup>\*,[a, b]</sup>

**Abstract:** The self-assembly and gelation behavior of a series of mono- and disubstituted ferrocene (Fc)–peptide conjugates as a function of ferrocene conformation and amino acid chirality are described. The results reveal that ferrocene–peptide conjugates self-assemble into organogels by controlling the conformation of the central ferrocene core, through inter- versus intramolecular hydrogen bonding in the attached peptide chain(s). The chirality controlled assembling studies showed that two monosubstituted Fc conjugates FcCO–LFLFLA-OMe and FcCO–LFLFDa-OMe form gels

with nanofibrillar network structures, whereas the other two diastereomers FcCO–dFLFLA-OMe and FcCO–LFDFLA-OMe exclusively produced straight nanorods and non-interconnected small fibers, respectively. This suggests the potential tuning of gelation behavior and nanoscale morphology by altering the chirality of constituted amino acids. The current study confirms the profound effect of diastereomerism and no influence of enantiomers on gelation. Correspondingly, the diastereomeric and enantiomeric Fc[CO–FFA-OMe]<sub>2</sub> were constructed for the study of chirality-organized structures.

## Introduction

Supramolecular gels are an important class of soft materials where gelator molecules assemble into three dimensional networks using noncovalent interactions.<sup>[1–9]</sup> In recent years, the self-assembly and gelation of low molecular mass organic molecules<sup>[10,11]</sup> including peptides<sup>[12–29]</sup> have attracted significant attention in the production of functional soft materials. Due to the reversible nature of interactions, these gels are responsive and tuneable. Responsiveness of these gels to stimuli such as light,<sup>[30–33]</sup> pH changes,<sup>[34]</sup> ultrasound,<sup>[35–37]</sup> enzymes<sup>[38,39]</sup> and changes in the redox state<sup>[40–43]</sup> is of particular interest. In order to design such “smart peptide materials”, it is important to have a thorough understanding of the intermolecular interactions that control the self-assembly and consequent architecture of the material and its bulk properties. However, at this point, the relation between the interactions and the resulting bulk material properties are not well understood. Hence, there is a growing interest in the design of molecules that undergo controlled and predictable self-assembly and gelation with

stimuli-responsiveness. Such systems are being studied due to fundamental scientific curiosity and numerous potential applications of smart and responsive materials.<sup>[4,6,8]</sup> For the construction of various molecular assemblies with tunable properties, the control of hydrogen bonding is an important tool by virtue of its directionality, specificity, reversibility and tuneability.<sup>[44–47]</sup> Chiral gels are of great interest, as molecular chirality can be translated into supramolecular chirality and nanoscale fibrillar architectures of gels.<sup>[48–53]</sup> It was recently reported that chirality of nanofibrous gels significantly influences cell adhesion and proliferation.<sup>[54]</sup> Chirality studies on gels are mostly confined to enantiomeric and racemic systems and the way chiral information is transformed and amplified into supramolecular assemblies.<sup>[48,49]</sup> However, there are only a few reports on the molecular chirality regulated tuning of gelation and nanostructures.<sup>[55–58]</sup> Smith and co-workers have shown that altering the chirality of one amino acid of a dendritic peptide organogelator can lead to changes in the gelation behavior in terms of fibrous nature.<sup>[56]</sup> However, the current understanding about the impact of chirality on peptide gelation and resulting nanostructures is limited and further investigation is required.

Conjugation of ferrocene (Fc) with peptides has been explored due to their interesting structural properties such as mimicking of protein secondary structures.<sup>[59–68]</sup> The distance between the two cyclopentadienyl rings of ferrocene molecule supports intramolecular hydrogen bonding between the attached peptide strands as observed in  $\beta$ -sheets. In our previous study, we hypothesized that peptides, upon conjugation to ferrocene (Fc), would be able to form an assembly which could react to changes in the redox state of Fc group.<sup>[69,70]</sup> In an attempt to test the applicability of our hypothesis, we pre-

[a] Dr. B. Adhikari, C. Singh, Dr. A. Shah, Prof. Dr. H.-B. Kraatz  
Department of Physical and Environmental Sciences  
University of Toronto, 1265 Military Trail, Toronto, M1C 1A4 (Canada)  
E-mail: bimalendu.adhikari@utoronto.ca  
bernie.kraatz@utoronto.ca

[b] Dr. A. J. Lough, Prof. Dr. H.-B. Kraatz  
Department of Chemistry, University of Toronto  
80 St. George Street, Toronto, Ontario M5S 3H6 (Canada)

[c] Dr. A. Shah  
Present address: Department of Chemistry  
Quaid-i-Azam University, 45320 (Pakistan)

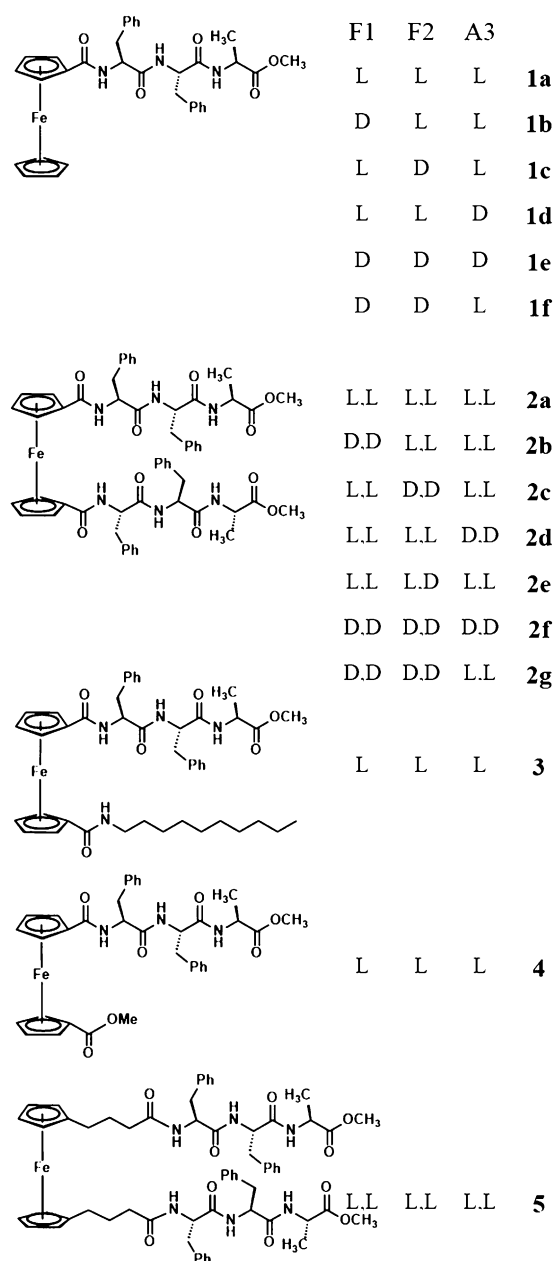
Supporting information for this article is available on the WWW under <http://dx.doi.org/10.1002/chem.201501395>.

pared a simple monosubstituted Fc-peptide conjugate and demonstrated redox responsiveness and a dramatic morphological change that alters the assembling behavior of the conjugate.<sup>[69,70]</sup> Herein, we further hypothesize that a modulation of interpeptide hydrogen bonding should allow us to influence self-assembly. Such modulation can be achieved, in principle, using 1,*n*'-disubstituted Fc-peptide conjugates, which can adopt a range of conformations as a consequence of intramolecular H-bonding that exists between the two podant peptide chains.<sup>[67,71]</sup> In addition, we speculate that potentially even changes in amino acid chirality may influence their ability to modulate the supramolecular aggregates. Due to the translation of amino acid spatial disposition to overall Fc-peptide conjugate and conformational changes, supramolecular assembly can be influenced. To demonstrate the applicability of our hypothesis, we set out to prepare a series of systems 1–5 (Scheme 1) and investigated their chirality and conformational regulated self-assembly and gelation.

## Results and Discussion

For this study, a short hydrophobic amyloid peptide sequence Aβ(19–21)-FFA, with self-assembling propensity was attached to ferrocene monocarboxylic acid FcCOOH (Fc-peptide conjugate 1), 1,1'-ferrocenedicarboxylic acid Fc[COOH]<sub>2</sub> (Fc-peptide conjugate 2), 1,*n*'-Fc[CO-NHC<sub>10</sub>H<sub>21</sub>][COOH] (Fc-peptide conjugate 3), Fc[COOMe][COOH] (Fc-peptide conjugate 4), Fc[C<sub>3</sub>H<sub>5</sub>-COOH]<sub>2</sub>, 1,1'-bis(3-propylcarboxylic acid)-ferrocene (Fc-peptide conjugate 5; Scheme 1). All target Fc-peptide conjugates were synthesized by using conventional solution-phase methodology. These were fully characterized using 1D (proton, carbon) and 2D NMR (gCOSY, gHMBCAD) spectroscopy as well as mass spectrometry (see the Supporting Information). In the first study, we discuss the ferrocene conformation guided self-assembly of Fc-peptide conjugates with homochiral peptide sequence LFLFLA (1a, 2a, 3, 4 and 5). Interestingly, Fc-peptide conjugate 1a, 3, 4 and 5 excluding Fc-peptide conjugate 2a were found to form gels.

Next, we investigated the impact of the chirality of each amino acid on the gelation and morphology of Fc-peptide conjugate FcCO-FFA-OMe (1) and for this purpose four diastereomers [FcCO-LFLFLA-OMe (1a), FcCO-DLFLFLA-OMe (1b), FcCO-LDFLFLA-OMe (1c) and FcCO-LFLFDLFLA-OMe (1d)] and two pairs of enantiomers [FcCO-LFLFLA-OMe (1a) and FcCO-DLFLFLA-OMe (1e); FcCO-LFLFDLFLA-OMe (1d) and FcCO-DLFLFDLFLA-OMe (1f)] were studied (Scheme 1). The results of Fc conjugates 1 established that gelation and morphologies are strongly influenced by diastereomeric effects whereas enantiomerism lacks these special characteristics. The effect of diastereomeric (2a–2e) and enantiomeric (2f–2g) changes on the conformation, chirality organized structure and morphologies in the Fc-peptide conjugate Fc[CO-FFA-OMe]<sub>2</sub> (2) was also studied.



**Scheme 1.** Chemical structures of monosubstituted Fc-peptide conjugates 1a–1f and the corresponding disubstituted Fc-peptides 2a–2g. Included in this study are also disubstituted Fc conjugates of the type Fc[CO-C10][CO-FFA-OMe] (3) possessing a peptide substituent on one of the Cp rings and an decylamide substituent on the other Cp ring, Fc[COOMe][CO-FFA-OMe] (4) possessing an ester group on one of the Cp rings and lastly Fc[C<sub>3</sub>-CO-FFA-OMe]<sub>2</sub> (5), an Fc system that possesses three-carbon long alkyl spacers to separate the peptide substituents from the Fc core. The chemical structures are shown on the left. Indicated on the right are the amino acid chiralities for each compound.

### Ferrocene conformation guided gelation

<sup>1</sup>H NMR spectroscopy was extensively used to recognize the H-bonding pattern and conformation of ferrocene peptides in solution that can provide insights about their self-assembling behavior.<sup>[58,63]</sup> All Fc-peptide conjugates (1–5) were fully charac-

terized using 1D and 2D NMR (gCOSY, gHMBCAD) spectroscopy in a non-gelling solvent  $\text{CDCl}_3$  as well as in a gelling solvent  $[\text{D}_8]\text{toluene}$  (see the Supporting Information). The NMR spectroscopy studies were performed at room temperature ( $22^\circ\text{C}$ ) for  $\text{CDCl}_3$  and at higher temperature ( $50^\circ\text{C}$ ) in the case of  $[\text{D}_8]\text{toluene}$  as some of the Fc-peptide conjugates remain in gel state at room temperature. It was noted that the Fc-peptide conjugates show a similar pattern of proton resonance in both solvents (Figure 1 for  $\text{CDCl}_3$  and Figure S1 in the Supporting Information for  $[\text{D}_8]\text{toluene}$ ), suggesting that they most likely have similar hydrogen-bonding patterns and conformation in both solvents.

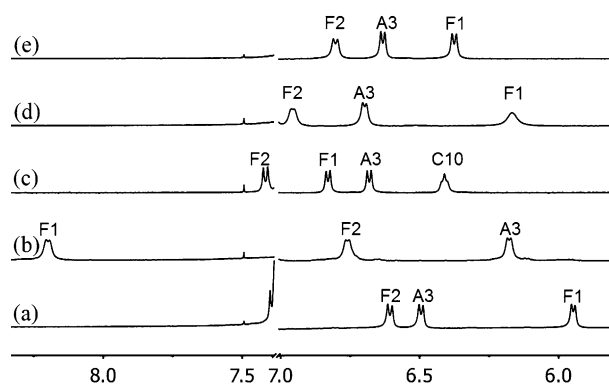


**Figure 1.**  $^1\text{H}$  NMR stack plots of different Fc-peptide conjugates ( $\text{CDCl}_3$ , 5 mm,  $22^\circ\text{C}$ ) displaying the amide region: a)  $\text{FcCO-LFLFLA-OMe}$  (**1a**), b)  $\text{Fc}[\text{CO-LFLFLA-OMe}]_2$  (**2a**), c)  $\text{Fc}[\text{CO-C10}][\text{CO-LFLFLA-OMe}]$  (**3**), d)  $\text{Fc}[\text{CO-OMe}][\text{CO-LFLFLA-OMe}]$  (**4**), and e)  $\text{Fc}[\text{C}_3\text{-CO-LFLFLA-OMe}]_2$  (**5**). The spectra show the relative positions of amide resonances of the same tripeptide (LFLFLA) in different compounds, presumably giving a clue of hydrogen bonding and differences in conformations. Indicated above the peaks are the corresponding amino acids for each compound.

Variable concentration NMR (VC-NMR) and variable-solvent NMR (VS-NMR) spectroscopies were performed to assess the nature of hydrogen bonding in different Fc-peptide conjugates. These NMR spectroscopy data are summarized in Table 1 and the corresponding spectra can be seen in Figure S2 in the Supporting Information.

For monosubstituted Fc-peptide conjugate **1a**, all three amide protons appear at  $\delta$  below 7 ppm in  $\text{CDCl}_3$  as well as in  $[\text{D}_8]\text{toluene}$ , which indicates the absence of intramolecular H bonds.<sup>[67,72]</sup> The chemical shifts of all the amide NH proton signals are both concentration- and solvent-dependent, suggesting the involvement of all amide protons in intermolecular H bonding (Figure 1, Table 1). Similarly, this establishes the presence of three intermolecular H bonds in Fc-peptide conjugate **4**. In case of disubstituted Fc-peptide conjugate **2a**, F1 NH appears much downfield,  $\delta = 8.20$  ppm, at room temperature, suggesting strong hydrogen bonding. The chemical shifts of the amide NH proton signals of F1 and A3 are concentration independent, whereas that of F2 is concentration-dependent. However, VS-NMR indicates that the amide proton signal of F1 is solvent-independent, whereas those of F2 and A3 are solvent-dependent, suggesting the involvement of F1 amide pro-

tons in intramolecular H bonding and F2 in intermolecular H bonding (Figure 1, Figure S2 in the Supporting Information, Table 1).

For disubstituted Fc-peptide conjugate **3**, F1 and F2 amides appear around  $\delta = 7$  ppm (in both  $\text{CDCl}_3$  and  $[\text{D}_8]\text{toluene}$ ), most likely suggesting the involvement of intramolecular hydrogen bonds. The proton NMR spectra in  $\text{CDCl}_3$  at RT show that both F1 and F2 NHs appear more downfield (almost equal magnitude) compared to monosubstituted Fc conjugate **1** as well as disubstituted Fc conjugate **4**. Both VC-NMR and VS-NMR spectra of Fc conjugate **3** show an almost equal magnitude shift in amide protons of F1 and F2, while the shift for A3 NH is higher than the other two amide protons. It is anticipated that both F1 and F2 amide protons are simultaneously hydrogen bonded with ferrocenyl  $\text{C}=\text{O}$  of the other strand, which is known as bifurcating intramolecular H bond.<sup>[73]</sup> Moreover, all aliphatic protons of C10 alkyl chain were more shifted up-field (0.4–0.5) than the ester  $\text{CH}_3$  (0.02) with an increase in temperature, suggesting the presence of van der Waals interactions between alkyl chains (Figure S3 in the Supporting Information).

Interestingly, in disubstituted Fc-peptide conjugate **5**, two peptide chains are attached to the ferrocene moiety with a three-carbon alkyl chain, all three amide protons resonate below  $\delta = 7$  ppm at room temperature. This indicates the absence of intramolecular H bonds and hence the absence of Herrick conformation. Moreover, the VC- and VS-NMR spectra confirm the presence of three intermolecular H bonds.

Next, it was crucial to investigate how differences in the hydrogen-bonding pattern affect the conformation around the ferrocene core. Therefore, circular dichroism (CD) was used for the elucidation of conformation and metallocene chirality of ferrocene peptide conjugates **1a**, **2a**, **3**, **4** and **5** (Figure 2).<sup>[62,67]</sup> CD of Fc-peptide conjugate **1a** (in chloroform) shows a very weak positive Cotton effect at 460 nm, which is expected for monosubstituted Fc-peptide. While, Fc conjugates **2a** and **3** exhibit a strong Cotton effect in the range of 480–490 nm, suggesting the presence of intramolecular interstrand hydrogen bonds, which results in axial chirality around the ferrocene core.<sup>[62,67]</sup> By combining the hydrogen-bonding pattern from the NMR spectra and CD results, we believe *P*-helical “Herrick” and “van Staveren”-like conformations are formed in Fc conjugate **2a** and **3**, respectively (Figure 2B). These results are well aligned with the NMR spectroscopy data which confirm the presence of intramolecular hydrogen bonds for both **2a** and **3**. Although, Fc conjugate **5** is a disubstituted system, interestingly it exhibits a very weak CD signal around the 450–500 nm region, suggesting the formation of an open conformation (“*Xu*” or *anti*) that does not adopt a typical structure by intramolecular hydrogen bonds between two peptide chains (Figure 2B).<sup>[67,71]</sup> The open conformation supports three intermolecular hydrogen bonds per peptide chain (by a sheet-like conformation) and this again supports the NMR spectroscopy studies. However, Fc conjugates **1a** and **4** show much enhanced CD signals in toluene presumably due to the formation of the self-assembled gel state that induces supramolecular chirality in the ferrocene region (vide infra and Figure S4 in the Supporting Information).

**Table 1.** NMR parameters of Fc-peptide conjugates of homochiral peptide sequence LFLFLA (1 a, 2 a, 3, 4 and 5) and evaluation of hydrogen bonding pattern in solution.

Residue	NH CDCl <sub>3</sub> ([D <sub>8</sub> ]Tol) <sup>[a]</sup>	$\Delta\delta$ -VC <sup>[b]</sup>	$\Delta\delta$ -VS <sup>[c]</sup>	Nature of H-bond <sup>[d]</sup>	Structure with H-bonding pattern
<b>FcCO-LFLFLA-OMe (1 a)</b>					
F1	5.95(5.96)	0.21	0.69	inter	
F2	6.63(6.80)	0.23	0.60	inter	
A3	6.51(6.42)	0.20	0.62	inter	
<b>Fc[CO-LFLFLA-OMe]<sub>2</sub> (2 a)</b>					
F1	8.20(8.22)	0.07	0.04	intra	
F2	6.76(6.84)	0.23	0.85	inter	
A3	6.18(6.38)	0.08	0.65	inter/no	
<b>Fc[CO-C10][CO-LFLFLA-OMe] (3)</b>					
F1	6.83(7.08)	0.02	0.22	intra	
F2	7.41(7.34)	0.02	0.31	intra	
A3	6.68(6.76)	0.05	0.37	inter	
<b>Fc[CO-OMe][CO-LFLFLA-OMe] (4)</b>					
F1	6.17(6.24)	0.09	0.6	inter	
F2	6.95(6.97)	0.10	0.5	inter	
A3	6.70(6.62)	0.10	0.58	inter	

In the course of our investigation of the self-assembly of Fc-peptide conjugates, it was found that the monosubstituted Fc-peptide conjugate, namely FcCO-LFLFLA-OMe (**1 a**), forms a gel (Figure 3). Then, we were curious to know whether the disubstituted Fc-peptide conjugates, Fc[CO-LFLFLA-OMe]<sub>2</sub> (**2 a**) and Fc[CO-C10][CO-LFLFLA-OMe] (**3**), would be able to form gels as they adopt intramolecularly hydrogen bonded 1,2'-"Herrick" and "van Staveren"-like conformations, respectively. Intriguingly, **2 a** did not form gel in a range of organic solvents. Whereas **3** forms gel with lower gelation efficiency than **1 a**, most likely indicating the role of van der Waals interactions for the introduction of a ten-carbon long alkyl chain in **3**. Then we came up with the idea of breaking the "Herrick" conformation by the introduction of a three-carbon long alkyl spacer in disubstituted Fc conjugate Fc[CO-C<sub>3</sub>-LFLFLA-OMe]<sub>2</sub> (**5**) which may

disrupt the intramolecular interchain H bonds adopting an open conformation and this leads to gelation in practice. Overall, the self-assembly of Fc-peptide conjugates with homochiral peptide (LFLFLA), including **1 a**, **3**, **4** and **5** formed gels while **2 a** did not form gel (Figure 3A).

Minimum gelation concentrations (mgc) of 0.12, 0.50, 0.38 and 0.40% w/v are found for gels obtained from **1 a**, **3**, **4** and **5**, respectively. Transmission electron microscopic studies of all four gels of Fc conjugates **1 a**, **3**, **4** and **5** show cross-linked nanofibrillar network morphology, that is responsible for entrapping many solvent molecules, giving rise to gel (Figure S5 in the Supporting Information). The Fc conjugate **2 a** produces isolated spheroids and no cross-linked network was found, which may be responsible for its non-gelling behavior (vide infra). In rheological studies, all gels exhibit storage modulus

Table 1. (Continued)					
Residue	NH CDCl <sub>3</sub> ([D <sub>8</sub> ]Tol) <sup>[a]</sup>	$\Delta\delta$ -VC <sup>[b]</sup>	$\Delta\delta$ -VS <sup>[c]</sup>	Nature of H-bond <sup>[d]</sup>	Structure with H-bonding pattern
Fc[C <sub>3</sub> -CO-LFLFLA-OMe] <sub>2</sub> (5)					
F1	6.37(-)	0.34	0.28	inter	
F2	6.80(7.56)	0.30	0.36	inter	
A3	6.63(6.34)	0.30	0.35	inter	

[a] Chemical shifts (ppm) of amide protons in CDCl<sub>3</sub> at a concentration of 5 mM at 22 °C. The values in parentheses correspond to those in [D<sub>8</sub>]Tol, at a concentration of 5 mM and 50 °C. [b]  $\Delta\delta$ -VC (variable concentration) means  $\Delta\delta = \delta(\text{CDCl}_3 \text{ at } 20 \text{ mM}) - \delta(\text{CDCl}_3 \text{ at } 5 \text{ mM})$  at 22 °C. [c]  $\Delta\delta$ -VS (variable solvent) means  $\Delta\delta = \delta(\text{CDCl}_3 + [\text{D}_8]\text{DMSO (20:1)}) - \delta(\text{CDCl}_3)$  at 5 mM concentrations and 22 °C. [d] The conclusions about the nature of hydrogen bonding are made by using the three sets of NMR spectroscopy data, where we followed three assumptions: 1) in case of disubstituted Fc-peptide systems, the presence of amide resonances above  $\delta = 7$  ppm in nonhydrogen-bonding solvents (CDCl<sub>3</sub> or [D<sub>8</sub>]toluene) suggests the presence of H-bonding and a "Herrick conformation" stabilized by two symmetrical intramolecular interstrand hydrogen bonds. 2) In the variable concentration NMR (VC-NMR) spectroscopy studies, an intermolecularly hydrogen bonded amide proton is much more affected than an intramolecularly hydrogen bonded amide proton. 3) An intermolecularly hydrogen bonded amide proton resonance is shifted much more than an intramolecularly hydrogen bonded amide proton during the addition of aliquots of [D<sub>8</sub>]DMSO to CDCl<sub>3</sub> (VS-NMR).

( $G'$ ) greater than loss modulus  $G''$ , indicating that they are effective physical gels.  $G'$  values for gels follow the order: **5** (20900 Pa) > **3** (5370 Pa) > **1a** (1270 Pa) > **4** (50 Pa) at an angular frequency of  $1 \text{ rad s}^{-1}$ , suggesting the strength of these gels follow the order **5** > **3** > **1a** > **4** (Figure 3B). Therefore, the tuning of gel strength may be achieved by manipulation of the gelator chemical structure.

In a detailed gelation study, Fc-peptide conjugate FcCO-LFLFLA-OMe (**1a**) self-assembles and forms a thermoreversible organogel in a range of organic solvents including toluene. The mgc was found to be 0.62% w/v for *p*-xylene, 0.07% w/v for cyclohexane, 0.12% w/v for toluene, 0.12% w/v for *o*-xylene, 0.21% w/v for *o*-dichlorobenzene and 0.33% w/v for ethyl ether. Therefore, gelation efficiency follows the following solvent order: *p*-xylene > cyclohexane > toluene > *o*-xylene > *o*-dichlorobenzene > ethyl ether and this matches with the Burdick and Jackson polarity index in descending order (cyclohexane 0.2 < toluene 2.4 < *o*-xylene 2.5 < *o*-dichlorobenzene 2.7 < ethyl ether 2.8). The gelation phenomenon was observed in the 0.2–2.8 range of polarity index. For instance, hexane and dichloromethane do not support gelation as their polarity indexes are either too low (0.1) or too high (3.1), respectively.

We tried to understand the gelation abilities of Fc-peptide conjugates (**1a**, **2a**, **3**, **4** and **5**) of a homochiral peptide LFLFLA in light of hydrogen-bonding pattern and conformation around the ferrocene core that are derived from NMR spectroscopy and CD studies (vide supra). NMR spectroscopy demonstrates that **1a** involves three intermolecular hydrogen bonds, **2a** involves "Herrick"-like conformation via one intra- and one intermolecular hydrogen bond per peptide chain, and **3** engages in one bifurcated intra- and one intermolecular hydro-

gen bond as well as van der Waals interactions. This leads to the formation of a super gel for **1a**, no gel for **2a**, and formation of a weak gel with lower efficiency for **3**. One intermolecular hydrogen bond and van der Waals interactions are responsible for gelation in Fc-peptide conjugate **3**. Incorporation of a three-carbon long alkyl chain, leads to the breaking of "Herrick" conformation in case of **5**, which allows the formation of three intermolecular hydrogen bonds per peptide chain, regaining its gelation abilities. This clearly exhibits that gel forming ability is directly proportional to the number of intermolecular hydrogen bonds and inversely proportional to the number of intramolecular hydrogen bonds. Moreover, intramolecularly hydrogen bonded "Herrick"-like conformation inhibits gel formation whereas an open conformation, that does not allow intramolecular hydrogen bonds, encourages gel formation. Therefore, we can control/design the gelation/gelator on the basis of intra- and versus intermolecular hydrogen-bond forming ability and conformation around the ferrocene core in Fc-peptide conjugates.

### Chirality controlled self-assembly

After having the result of ferrocene conformation guided dramatic change in gelation and morphological behavior between monosubstituted ferrocene-peptide conjugates FcCO-FFA-OMe (**1**) and the corresponding disubstituted Fc[CO-FFA-OMe]<sub>2</sub> (**2**), we planned to investigate the self-assembly as a function of amino acid chirality in **1** and **2** as the change in chirality can lead to the change in molecular conformation and hence self-assembly and gelation. For Fc-peptide conjugate **1**, four diastereomers (**1a–d**) and two pairs of enantiomers (**1a–1e** and

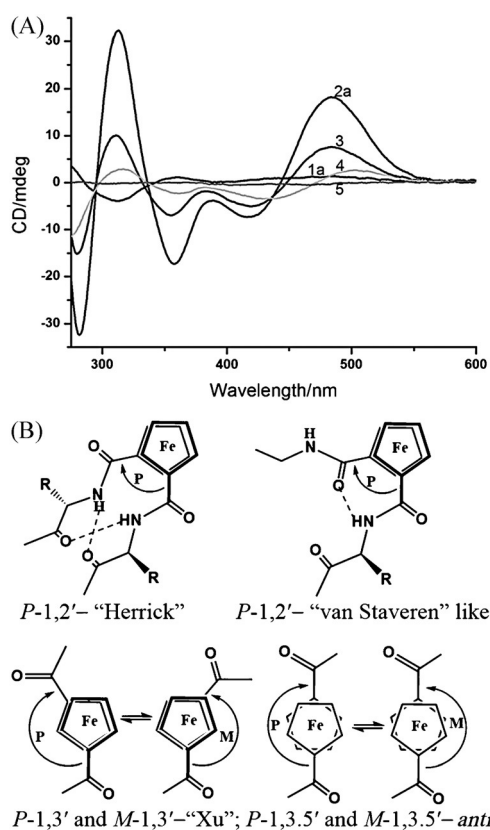


**Figure 2.** A) CD spectra of different Fc-peptide conjugates of homochiral peptide (LFLFLA) in chloroform (5 mm, 22 °C, cell length 1.0 mm) for the evaluation of their conformations around the ferrocene core. The high ellipticity values for Fc-peptide conjugates **2a** and **3** suggest the formation of an intramolecularly hydrogen bonded conformation to induce helical chirality of ferrocene. B) The illustrations for the different conformations of disubstituted ferrocene peptide conjugates: *P*-1,2'-"Herrick", *P*-1,2'-"van Staveren"-like, *P*-1,3' and *M*-1,3.5'-"Xu" and *P*-1,3.5' and *M*-1,3.5'-*anti* conformations. The "Herrick" conformation is stabilized by two intramolecular interstrand hydrogen bonds whereas "van Staveren" is stabilized by one intramolecular interstrand hydrogen bond. The two cyclopentadienyl rings cannot rotate in "Herrick" and "van Staveren"-like conformations as they are locked by intramolecular hydrogen bonds. On the other hand, there is no intramolecular hydrogen bond in the two open conformations ("Xu" and *anti*) resulting in racemization of metallocene chirality.

**1d–1f**) were studied to see the differences of their self-assembly, gelation and morphology. The comparative NMR spectra of all four diastereomers show the appearance of three amide protons in different positions, indicating the significant differences in their conformation that might be responsible for their macroscopic behavior (Figure 4A).

To understand the differences in self-assembling behavior, we explored the hydrogen-bonding pattern by VC- and VS-NMR spectroscopy studies (see Figure S6 for the spectra and Table S1 for summarized data in the Supporting Information). The results suggest that the two F amides are involved in intermolecular hydrogen bonding and A3 NH may have inter-/intra-/no hydrogen bond for three heterochiral Fc-peptide conjugates **1b–d**, indicating they also self-associate in solution. CD spectra of diastereomeric Fc-peptide conjugates **1a–d** in toluene suggest a significantly enhanced CD signal in toluene for two gelator conjugates (**1a** and **1d**) than non-gelator pep-

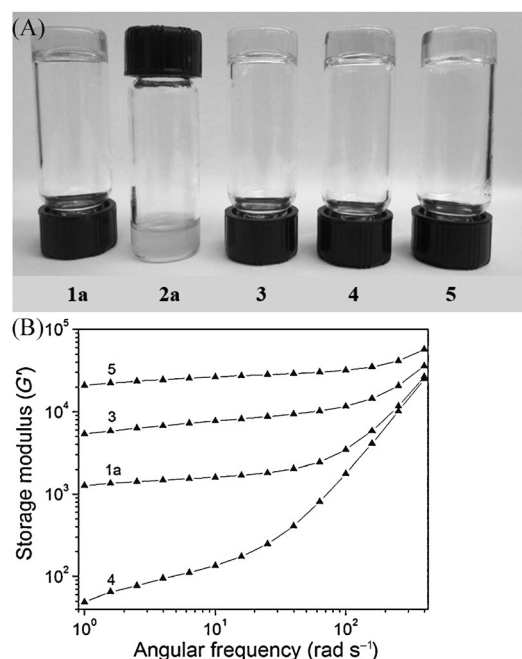


**Figure 3.** A) Gelation test of Fc-peptide conjugates of homochiral peptide LFLFLA (**1a**, **2a**, **3**, **4** and **5**) in toluene at 5 mm concentration, where all conjugates form gel excluding **2a**, presumably indicating the role of the conformation around the ferrocene core. Inverted vials indicate gels whereas the non-inverted vial indicates the non-gel state. B) The frequency sweep experiments of gels (0.5%, w/v) as indicated in the figure. The strength of the gels are evaluated in terms of storage modulus ( $G'$ ) values obtained from the plot.

ptide conjugates (**1b** and **1c**), whereas four diastereomers do not significantly differ in chloroform (Figure 5A–C and Figure S7 in the Supporting Information). This is presumably due to the formation of supramolecular chirality in gel state for two (**1a** and **1d**) diastereomers (vide infra gelation studies). In a temperature-dependent CD study (Figure 5C), the ferrocene signals almost approached the base-line at an elevated temperature (80 °C), where gelator molecules remain in the solution state and are most likely not in the self-assembled state. This clearly suggests the room temperature enhanced CD signal is a consequence of supramolecular chirality rather than inherent molecular chirality.<sup>[49,50]</sup> Moreover, the Fc-based CD signals differ significantly for two gels of **1a** and **1d**, indicating the differences in their self-assembling pattern in toluene (Figure 5A).

Similarly, to understand the role of each amino acid chirality in the disubstituted Fc-peptide conjugate **2** on the resultant conformation, helically organized structure and morphology, five diastereomers, namely Fc[CO-LFLFLA-OMe]<sub>2</sub> (**2a**), Fc[CO-DFLFLA-OMe]<sub>2</sub> (**2b**), Fc[CO-LFdFLA-OMe]<sub>2</sub> (**2c**), Fc[CO-LFLFdA-OMe]<sub>2</sub> (**2d**) and Fc[CO-LFdFLA-OMe][CO-LFLFLA-OMe] (**2e**) were studied, where the first four diastereomers have two symmetrical peptide chains and the last diastereomer has two nonsymmetrical peptide chains. We also investigated two sets of enantiomers, namely Fc[CO-LFLFLA-OMe]<sub>2</sub> (**2a**) versus Fc[CO-DFdFdA-OMe]<sub>2</sub> (**2f**) and Fc[CO-LFLFdA-OMe]<sub>2</sub> (**2d**) versus Fc[CO-DFdFLA-OMe]<sub>2</sub> (**2g**).

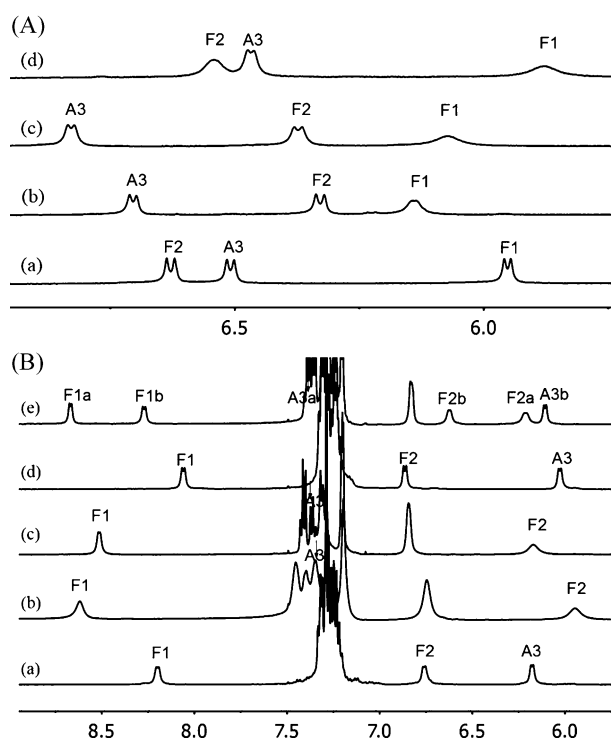


**Figure 4.**  $^1\text{H}$  NMR stack plots ( $\text{CDCl}_3$ , 5 mm,  $22^\circ\text{C}$ ) displaying the amide region: A) Four monosubstituted diastereomeric Fc-peptide conjugates **1a–d**: a) FcCO–LFLFLA–OMe (**1a**), b) FcCO–DFLFLA–OMe (**1b**), c) FcCO–LFDFLA–OMe (**1c**), and d) FcCO–LFLFLA–OMe (**1d**); B) Five disubstituted diastereomeric Fc-peptide conjugates **2a–e**: a) Fc[CO–LFLFLA–OMe] $_2$  (**2a**), b) Fc[CO–DFLFLA–OMe] $_2$  (**2b**), c) Fc[CO–LFDFLA–OMe] $_2$  (**2c**), d) Fc[CO–LFLFLA–OMe] $_2$  (**2d**), and e) Fc[CO–LFDFLA–OMe][CO–LFLFLA–OMe] (**2e**) showing the relative positions of amide resonances in different Fc conjugates. This presumably gives a clue to intramolecular hydrogen bonding and differences in conformations from one diastereomer to another. The top of the peaks are assigned to the corresponding amino acids for each compound.

The presence of either or both inter- and intramolecular hydrogen bonding and the resultant conformations were investigated thoroughly by NMR spectroscopy experiments described in Figure 4, Figure S8 in the Supporting Information and Table 2. The nature of hydrogen bonding for Fc-peptide conjugate Fc[CO–LFLFLA–OMe] $_2$  (**2a**) is already established (vide supra). The following conclusions are made from the comparison of the NMR spectroscopy studies (Figure 4). 1) For all four diastereomers, the very high downfield  $\delta$  value for F1 NH above 8 ppm suggests the presence of strong hydrogen bonds. 2) The appearance of A3 NH above 7 ppm for the two isomers Fc[CO–DFLFLA–OMe] $_2$  (**2b**) and Fc[CO–LFDFLA–OMe] $_2$  (**2c**) indicates its involvement in strong hydrogen bonding; 3) **2a** and **2d** possibly have similar conformations whereas **2b** and **2c** have similar structural pattern.

In VC- and VS-NMR spectroscopy experiments, two isomers **2b** and **2c** show the involvement of two intramolecular hydrogen bonds via F1 and A3 amide protons. It is noted that F1 NH appeared much more downfield (more than 1 ppm) than A3 NH, suggesting that it forms much stronger intramolecular hydrogen bond than A3. Based on these observations, we assume these two Fc-peptides adopt 1,2-Herrick conformation (stabilized by two symmetrical intramolecular interstrand hy-

drogen bonds via F1 amides) and  $\beta$ -turn-like conformation that is stabilized by two symmetrical intramolecular intrastrand hydrogen bonds via A3 amide protons (Table 2). In case of **2a** and **2d**, the VC- and VS-NMR spectroscopy experiments prove F1 NH and F2 NH participate in intra- and intermolecular hydrogen bonds, respectively, whereas A3 NH may hold intermolecular hydrogen bonds.

In the case of diastereomer Fc[CO–LFDFLA–OMe][CO–LFLFLA–OMe] (**2e**) having two nonsymmetrical peptide chains, two kinds of resonances were observed for every amide proton. Two F1 amide protons appeared at  $\delta=8.67$  and  $8.27$  ppm, suggesting they are involved in strong intramolecular hydrogen bonding. Interestingly, two A3 amide protons appeared at  $\delta=7.38$  and  $6.11$  ppm, suggesting that only one of the A3 amide protons ( $\delta=7.38$  ppm) occupies intramolecular hydrogen bonds. Both F2 amide protons resonate below  $\delta=7$  ppm, and the concentration and solvent dependency confirms their participation in intermolecular hydrogen bonds (Table 2 and Figure S8 in the Supporting Information).

The CD spectra of isomers of **2** are shown in Figure 5D–F and Figure S9 in the Supporting Information, and suggest the following: 1) each diastereomer shows a strong Cotton effect near 485 nm, suggesting the formation of intramolecularly hydrogen bonded “Herrick”-like conformation in solution; 2) the chirality of the first amino acid dictates the overall metallocene chirality; 3) the two enantiomeric pairs **2a** versus **2f** and **2d** versus **2g** show mirror image CD signals (Figure 5E); 4) the temperature independence suggests the strong CD signal in the ferrocene region is a consequence of induced molecular chirality and not due to supramolecular chirality (Figure 5F).

Single crystals suitable for X-ray analysis were obtained for two diastereomers of Fc-peptide conjugate **2**, namely **2b** and **2c**. Conjugate **2c** crystallized from toluene, a solvent used for gelation and self-assembly studies for all Fc-peptide conjugates. X-ray crystallography of **2c** reveals the presence of two crystallographically independent molecules that display significant differences in dihedral angles, thus reflecting differences in conformation (Figure 6A; Figure S10 and Table S2 in the Supporting Information). The ORTEP diagrams for one molecule is depicted in Figure 6A. In the molecule, the peptide substituents are in the 1 and 2' positions and intramolecular interstrand hydrogen bonded between the F1 C=O of one strand and F1 NH on the other strand ( $d[\text{N}(1\text{A})\cdots\text{O}(7\text{A})]=2.896(3)$  Å and  $d[\text{N}(4\text{A})\cdots\text{O}(2\text{A})]=3.119(3)$  Å for molecule A). Consequently, a 10-membered H-bonded ring is formed, and this structural pattern is known as the “Herrick conformation”.<sup>[67]</sup> In addition, there are also two symmetrical intramolecular intrastrand hydrogen bonds between amide NH of A3 and ferrocenyl C=O of the same strand ( $d[\text{N}(6\text{A})\cdots\text{O}(6\text{A})]=3.129(3)$  Å and  $d[\text{N}(3\text{A})\cdots\text{O}(1\text{A})]=3.024$  Å for molecule A) to form 10-membered H-bonded rings, and this results in a  $\beta$ -turn-like structure in each dipeptide chain. The torsion angles  $\varphi_2=-61.5^\circ$  ( $\varphi_2^*=-61.4^\circ$ ),  $\psi_2=134.9^\circ$  ( $\psi_2^*=141.2^\circ$ ),  $\varphi_3=93.3^\circ$  ( $\varphi_3^*=100.5^\circ$ ) and  $\psi_3=-6.8^\circ$  ( $\psi_3^*=-10.2^\circ$ ) for molecule A suggest a type II  $\beta$ -turn-like structure in spite of  $\varphi_2=-60^\circ$ ,  $\psi_2=120^\circ$ ,  $\varphi_3=80^\circ$  and  $\psi_3=0^\circ$  for an ideal type II  $\beta$ -turn.<sup>[74]</sup> In addition to the intramolecular hydrogen bonds, there are also intermolecular hy-

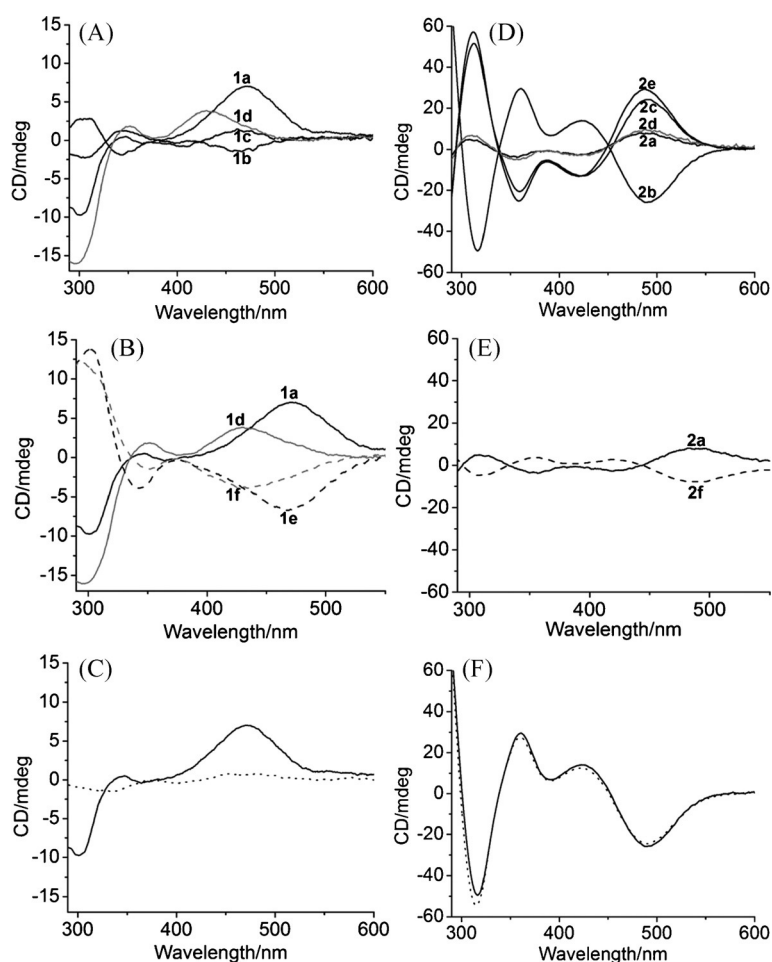


**Figure 5.** A–C) CD spectra for Fc-peptide conjugates **1** (toluene, 5 mm, at 22 °C, cell length 1.0 mm). A) Diastereomeric effect as indicated **1a–1d**. Enhanced CD signals in the ferrocene region are observed for two gelator conjugates (**1a** and **1d**) presumably indicating the formation of supramolecular chirality driven by gelation. B) Enantiomeric effect showing their mirror-image relationship. C) Temperature effect: (—) **1a** at 22 °C versus (.....) **1a** at 80 °C confirming the presence of supramolecular chirality.<sup>[49,50]</sup> D–E) CD spectra for Fc-peptide conjugates **2** (toluene, 5 mm, at 22 °C, cell length 1.0 mm). D) Diastereomeric effect as indicated **2a–2e**. All diastereomers of Fc-peptide conjugate **2** show a strong Cotton effect in the ferrocene region suggesting the formation of induced ferrocene chirality which arises from an intramolecularly hydrogen-bonded “Herrick”-like conformation in solution. E) Enantiomeric effect. F) Temperature effect: (—) **2a** at 22 °C versus (.....) **2a** at 80 °C confirming the presence of molecular chirality.

drogen-bond interactions between the NH of F2 and C=O on the F2 of the other molecule ( $d[\text{N}(5\text{A})\cdots\text{O}(3\text{B})]=2.900(3)\text{ \AA}$ ) at the supramolecular level (Figure S11 in the Supporting Information). These hydrogen-bonding interactions in the solid state match well with our findings of hydrogen-bonding patterns in solution from NMR spectroscopy studies (vide supra). The dihedral angle ( $\omega$ ) between the two ring-bound substituents is  $68^\circ$  for molecule A, which suggests *P*-1,2' “Herrick conformation”. This is in good agreement with the strong CD signal of Fc-peptide conjugate **2c** (vide supra).

Conjugate **2b** crystallized from toluene/dichloromethane solvent mixture and had an orthorhombic space group  $P2_12_12_1$  (Table S2 in the Supporting Information). It also showed “Herrick conformation” consisting of two intramolecular interstrand hydrogen bonds ( $d[\text{N}(1)\cdots\text{O}(7)]=3.017(10)\text{ \AA}$  and  $d[\text{N}(4)\cdots\text{O}(2)]=2.823(9)\text{ \AA}$ ) (Figure 6B). In contrast to **2c**, crystal

structure of **2b** displays only one intramolecular intrastrand hydrogen bond between amide NH of A3 and ferrocenyl C=O of the same strand ( $d[\text{N}(6\text{A})\cdots\text{O}(6\text{A})]=3.047(10)\text{ \AA}$ ) to nucleate a  $\beta$ -turn-like structure in each dipeptide chain. The torsion angles  $\varphi_2=61.5^\circ$ ,  $\psi_2=-140.5^\circ$ ,  $\varphi_3=-105.8^\circ$  and  $\psi_3=31.6^\circ$  suggest a type II'  $\beta$ -turn like structure. The other peptide chain involves in hydrogen bonding with solvent molecule dichloromethane. There are also intermolecular hydrogen-bonding interactions between the NH of F2 and C=O of A3 ( $d[\text{N}(2)\cdots\text{O}(6)]=2.811(9)\text{ \AA}$  and  $d[\text{N}(6)\cdots\text{O}(3)]=3.001(12)\text{ \AA}$ ; Figure S12 in the Supporting Information). However, **2b** forms similar conformation like **2c** in solution (vide supra). The crystal structure of **2b** shows a dihedral angle ( $\omega$ )  $73.5^\circ$  suggesting *P*-1,2' “Herrick conformation” and matches well with the CD result (vide supra). Moreover, a number of structural parameters and some specific angles such as the tilt angles ( $\theta$ ), dihedral angles ( $\omega$  and  $\beta$ ) can be seen in the supporting information (Figure S13 and Table S3 in the Supporting Information).

These results indicate that symmetrical introduction of two peptide chains with the first two amino acids of opposite chirality (DFLFLA or LFDFLA) onto the ferrocene scaffold as a central reverse-turn unit favours type II  $\beta$ -turn structure and “Herrick conformation” simultaneously. Whereas peptide chains with the first two amino acids of homochirality (LFLFLA or DFDFDA) onto the ferrocene scaffold only supports “Herrick conformation”.

The  $\beta$ -turn is the motif observed in folded proteins with proline and glycine are commonly observed amino acids at  $i+1$  or  $i+2$  positions of  $\beta$ -turns. Only a few peptide fragments DPro-Gly, DPro-Pro, DPro-Aib, Aib-DPro, Asp-Gly, DPh-Gly, Aib-DAla and others are known to induce  $\beta$ -turn conformation in pure peptide systems.<sup>[74–80]</sup> Previously, Hirao and coworkers reported type II  $\beta$ -turn-like structures for two dipeptide chains of heterochiral sequence LAla-DPro-NHPy or DAla-LPro-NHPy attached to the ferrocene scaffold.<sup>[81]</sup> We are the first to report that a new peptide fragment of heterochiral sequences LPh-DPh and DPh-LPh can potentially induce type II  $\beta$ -turn and

**Table 2.** NMR spectroscopy parameters for diastereomeric Fc-peptide conjugates **2b–e** for the evaluation of hydrogen-bonding patterns in solution. Data for the first disubstituted Fc-peptide conjugate **2a** are given in Table 1 and the other two Fc-peptide conjugates **2f** and **2g** showed identical chemical shifts with their enantiomeric Fc-peptide conjugates **2a** and **2d**, respectively, and hence they are omitted in this Table.

Residue	NH CDCl <sub>3</sub> ([D <sub>2</sub> ]Tol) <sup>[a]</sup>	$\Delta\delta$ -VC <sup>[b]</sup>	$\Delta\delta$ -VS <sup>[c]</sup>	Nature of H-bond <sup>[d]</sup>	Structure with H-bonding pattern
Fc[CO-dFLFLA-OMe] <sub>2</sub> ( <b>2b</b> )					
F1	8.62(8.63)	-0.01	-0.07	intra	
F2	5.95(5.77)	0.03	1.37	inter/no	
A3	7.35(5.77)	0.01	0.16	intra	
Fc[CO-lFdFLA-OMe] <sub>2</sub> ( <b>2c</b> )					
F1	8.55(8.62)	0.03	-0.01	intra	
F2	6.50(6.49)	0.09	1.47	inter/no	
A3	7.41(7.75)	0.08	0.14	intra	
Fc[CO-lFLFdA-OMe] <sub>2</sub> ( <b>2d</b> )					
F1	8.06(7.99)	0.06	0.03	intra	
F2	6.87(7.18)	0.20	0.69	inter	
A3	6.03(6.42)	0.06	0.66	inter/no	
Fc[CO-lFdFLA-OMe][CO-lFLFLA-OMe] ( <b>2e</b> )					
F1a	8.67(8.65)	0.1	-0.05	intra	
F2a	6.22(6.48)	0.2	1.47	inter	
A3a	7.38(7.60)	0.04	0.19	intra	
F1b	8.27(8.41)	0.05	0.06	intra	
F2b	6.62(7.05)	0.31	1.21	inter	
A3b	6.11(6.32)	0.1	0.80	inter/no	

[a] Chemical shifts (ppm) of amide protons in CDCl<sub>3</sub> at a concentration of 5 mM at 22 °C. The values in parentheses correspond to those in [D<sub>2</sub>]Tol, at a concentration of 5 mM and 50 °C. [b]  $\Delta\delta$ -VC (variable concentration) means  $\Delta\delta = \delta(\text{CDCl}_3 \text{ at } 20 \text{ mM}) - \delta(\text{CDCl}_3 \text{ at } 5 \text{ mM})$  at 22 °C. [c]  $\Delta\delta$ -VS (variable solvent) means  $\Delta\delta = \delta(\text{CDCl}_3 + [\text{D}_2]\text{DMSO (20:1)}) - \delta(\text{CDCl}_3)$ ; at 5 mM concentration and 22 °C. [d] The nature of hydrogen bonding was interpreted from proton NMR spectroscopy, variable concentration and solvent NMR spectroscopy data.

type II'  $\beta$ -turn structures in Fc-peptide conjugates Fc[CO-lFdFLA-OMe]<sub>2</sub> and Fc[CO-dFLFLA-OMe]<sub>2</sub> respectively.

The gelation abilities of different isomers for Fc conjugates **1** and **2** are presented in Figure 7A and B. Interestingly, only two Fc conjugates **1a** and **1d** form gel among four diastereomers, suggesting the potential diastereomeric effect on the self-assembling process and gelation. Other Fc-peptide conjugates **1b** and **1c** are unable to form gel and remain soluble in toluene. In addition, Fc-peptide conjugate **1d** showed better

gelation ability (of 0.7%, w/v mgc) than **1a** (with mgc 1.2%, w/v). A comparative rheological experiment exhibits the  $G'$  value of **1d** gel is greater than **1a** gel, suggesting the hetero chiral peptide gel is stronger than homochiral peptide gel (Figure 7B). However, **1e** and **1f** show almost similar gelation behaviours with **1a** and **1d** respectively, suggesting enantiomers do not affect gelation behavior. Conclusively, it is observed that the terminal first two amino acids (F1 and F2) have to be homo-chiral for gelation in this case. On the other hand, none

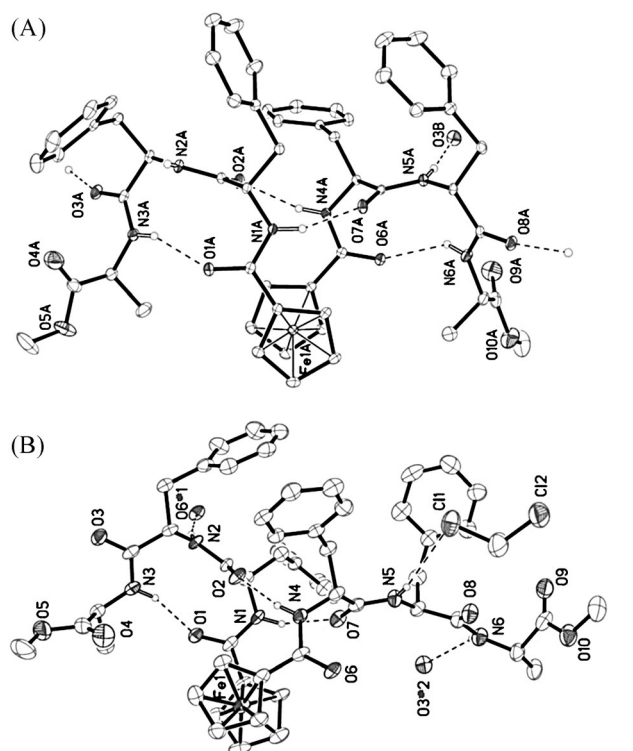


**Figure 6.** A) ORTEP diagram of molecule A of  $\text{Fc}[\text{CO-LFdFLA-OMe}]_2$  (**2c**) showing two intramolecular interstrand hydrogen-bonds ( $d[\text{N}(1\text{A})\cdots\text{O}(7\text{A})] = 2.896(3)$  Å and  $d[\text{N}(4\text{A})\cdots\text{O}(2\text{A})] = 3.119(3)$  Å), two intramolecular intrastrand hydrogen bonds ( $d[\text{N}(6\text{A})\cdots\text{O}(6\text{A})] = 3.129(3)$  Å and  $d[\text{N}(3\text{A})\cdots\text{O}(1\text{A})] = 3.024$  Å) and one intermolecular hydrogen bond ( $d[\text{N}(5\text{A})\cdots\text{O}(3\text{B})] = 2.900(3)$  Å). B) ORTEP diagram of  $\text{Fc}[\text{CO-DFLFLA-OMe}]_2$  (**2b**) showing two intramolecular interstrand hydrogen bonding ( $d[\text{N}(1)\cdots\text{O}(7)] = 3.017(10)$  Å and  $d[\text{N}(4)\cdots\text{O}(2)] = 2.823(9)$  Å), one intramolecular intrastrand hydrogen bond ( $d[\text{N}(6\text{A})\cdots\text{O}(6\text{A})] = 3.047(10)$  Å) and three intermolecular hydrogen bonds ( $d[\text{N}(2)\cdots\text{O}(6)\#1] = 2.81(9)$  Å,  $d[\text{N}(6)\text{-H}(6\text{A})\cdots\text{O}(3)\#2] = 3.00(12)$  Å and  $d[\text{N}(5)\text{-H}(5\text{A})\cdots\text{Cl}(1)] = 3.788(10)$  Å). The intramolecular and intermolecular hydrogen-bonding interactions are shown by dash (----) and dotted (.....) lines, respectively. Thermal ellipsoids are depicted at 30% probability. H atoms bonded to C atoms are not shown, and the H-bond acceptor O atoms are labeled.

of the isomers of Fc conjugates **2** forms gel. This is due to the fact that all of them form "Herrick" conformation involving intra-molecular hydrogen bonds which result in lack of enough inter-molecular hydrogen bonds that could cause gelation.

The morphologies of self-assembled diastereomeric Fc-peptide conjugates were characterized using transmission electron microscopy (Figure 8 and Figure S14 in the Supporting Information). Two gelator Fc-peptide conjugates **1a** and **1d** show cross-linked nanofibrillar network morphology that can effectively entrap a lot of solvent molecules, giving rise to gel formation. The average widths of these fibers are 70 nm and 30 nm respectively. In contrast, two non-gelator Fc-peptide conjugates **1b** and **1c** exhibit exclusively nanorod and small irregular fibers (that are not interconnected) in toluene, respectively. The nanorods have width of 200 nm and length of few micrometers on average indicating a high aspect ratio. The small fibers for **1c** are average 100 nm in width and average 1 µm in length. The differences in the morphologies of diastereomers are due to the differences in their self-assembly, as

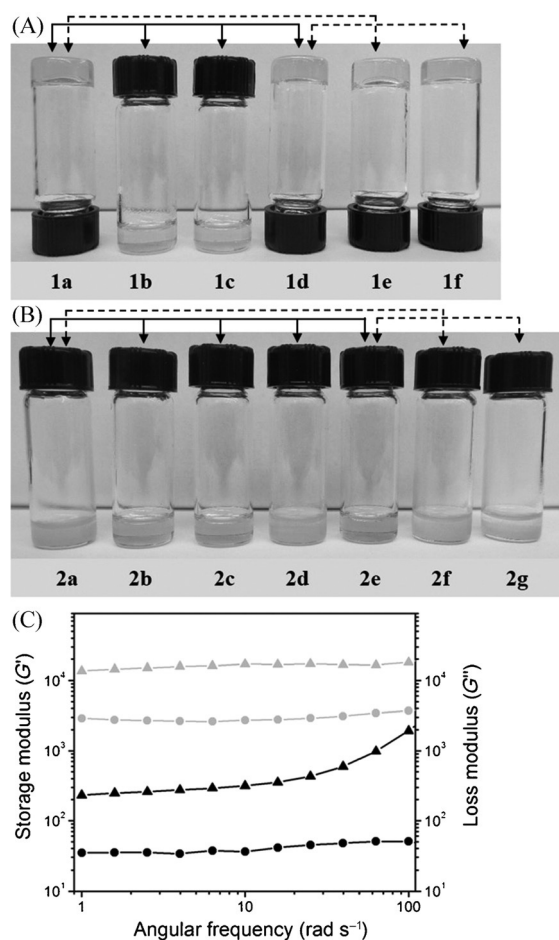


**Figure 7.** A, B) Photographs of chirality-guided gelation test for mono- and disubstituted Fc-peptide conjugates **1** and **2** in toluene at 5 mM concentration. Inverted vials correspond to gels whereas non-inverted vials to non-gel state. Solid arrows indicate diastereomeric relation whereas dashed arrows suggest enantiomeric relation among different conjugates. C) Frequency sweep experiments to measure the storage modulus (triangles) and loss modulus (circles) values for gels obtained from two diastereomeric Fc-peptide conjugates **1a** (black) and **1d** (light gray), respectively.

highlighted by TEM studies. Therefore, the tuning of nanoscale morphology is possible just by altering the amino acid chirality in diastereomers. However, the other two gelator Fc-peptide conjugates **1e** and **1f** showed identical nanofibrillar morphology with their enantiomeric Fc-peptide conjugates **1a** and **1d** respectively, suggesting enantiomers do not differ in nanoscale morphology (Figure S14 in the Supporting Information). In addition, the nanostructures have higher width than the molecular dimension of any Fc-peptide conjugates, suggests there is a self-association of several molecular chains to produce the supramolecular nanoscale structures.

Moreover, the diastereomeric Fc-peptide conjugates **2** mostly produce spheroid morphology with varying sizes. In case of **2a**, spheroids are in the range of 270 to 445 nm with an average diameter of 360 nm, while the spheroids are bigger for **2c** with an average size of 620 nm. However for **2d**, spheroids are interconnected to each other and sizes are relatively small with an average diameter of 290 nm. **2b** does not exhibit any ordered morphology in toluene. However, the other two

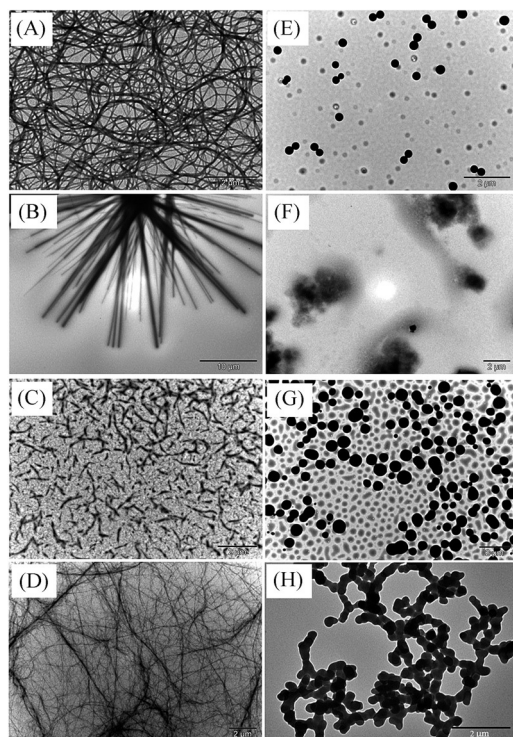


**Figure 8.** TEM images of diastereomeric Fc-peptide conjugates of **1** (A–D) and **2** (E–H) showing their self-assembled structures in toluene. Images of monosubstituted Fc-peptide conjugates of **1** show dramatic change in self-assembled structures from one diastereomer to the other: A) FcCO-LFLFLA-OMe (**1a**), B) FcCO-DFLFLA-OMe (**1b**), C) FcCO-LFDFLA-OMe (**1c**), and D) FcCO-LFLFDA-OMe (**1d**). Disubstituted Fc-peptide conjugates of **2** suggest they mostly form spheroid morphologies with varying sizes: E) Fc[CO-LFLFLA-OMe]<sub>2</sub> (**2a**), F) Fc[CO-DFLFLA-OMe]<sub>2</sub> (**2b**), G) Fc[CO-LFDFLA-OMe]<sub>2</sub> (**2c**), and H) Fc[CO-LFLFDA-OMe]<sub>2</sub> (**2d**). The scale bars are 2 μm for all images except for (B) which is 10 μm.

Fc-peptide conjugates **2f** and **2g** showed similar morphology with their enantiomeric Fc-peptide conjugates **2a** and **2d** (Figure S15 in the Supporting Information).

## Conclusion

Fc conjugate FcCO-LFLFLA-OMe (**1a**) self-assembles into sheet-like conformation via three intermolecular hydrogen bonds leading to the formation of a super-gel. In contrast, for Fc[CO-LFLFLA-OMe]<sub>2</sub> (**2a**), the symmetrical introduction of two peptide chains of LFLFLA into the ferrocene scaffold induces a “Herrick”-like conformation via two intramolecular interchain hydrogen bonds that prohibit gel formation due to lack of enough intermolecular hydrogen bonds, as required for gelation. Although, Fc[CO-C10][CO-LFLFLA-OMe] (**3**) adopts a “van Staveren”-like conformation which involves one bifurcated intramolecular hydrogen bond, the presence of a single intermolecular hydrogen bond and additional van der Waals interactions among the ten-carbon long alkyl chain causes gel formation. Interestingly, the introduction of a three-carbon long alkyl spacer in the disubstituted Fc conjugate Fc[CO-C<sub>3</sub>-LFLFLA-OMe]<sub>2</sub> (**5**) disrupts the intramolecular interchain H bonds and adopts an open conformation. This supports the formation of

three intermolecular hydrogen bonds per peptide chain retaining the gelation property. Therefore, ferrocene may serve as a reliable organometallic scaffold for the construction and tuning of organogels by controlling the conformation of the ferrocene core and proper conjugation of peptide segment(s). Consequently, the number of intermolecular hydrogen bonds increases gelation ability, while the presence of intramolecular hydrogen bonds decrease the gelation capability. Moreover, intramolecularly hydrogen bonded “Herrick”-like conformation inhibits gel formation whereas an open conformation, which does not allow intramolecular hydrogen bonds, assists gelation. Morphological studies of **1a**, **3**, **4** and **5** gels exhibit cross-linked nanofibrillar networks required for gelation, while Fc conjugate **2a**, in contrast has non-gelation behavior which is related to non-interconnected spheroid morphology. Hence, we can modulate the gelation properties and nanoscale architectures based on intra- and/or intermolecular hydrogen bonds and the conformation around the ferrocene core in Fc-peptide conjugates.

Chirality-guided gelation studies on monosubstituted Fc conjugates FcCO-FFA-OMe (**1**) established the dramatic role of diastereomeric effects on gelation, whereas enantiomers showed no impact on gelation. Two diastereomeric gelator Fc-peptide conjugates **1a** and **1d** showed cross-linked nanofibrillar networks, whereas two non-gelator Fc-peptide conjugates **1b** and **1c** produced nanorods and small irregular fibers, respectively, in toluene, suggesting the potential tuning of nanoscale morphology by simply altering the chirality of constituent amino acids.

NMR and CD spectroscopy studies of diastereomeric Fc conjugates **2** suggest that the symmetrical introduction of two peptide chains with the first two amino acids of opposite chirality (DFLFLA or LFDFLA) to the ferrocene scaffold favors β-turn structure and “Herrick conformation” simultaneously. Whereas peptide chains with the first two amino acids of homochirality (LFLFLA or LFLFDA) onto the ferrocene scaffold only supports “Herrick conformation”. Regarding the β-turn mimicking peptide segment, proline and glycine are the most commonly observed amino acids at *i*+1 or *i*+2 positions of β-turns. In this study, we report a new peptide fragment without proline and glycine residues for the first time, wherein sequences LFLF and DFLF can potentially induce type II β-turn and type II' β-turn structures in Fc-peptide systems Fc[CO-LFDFLA-OMe]<sub>2</sub> (**2c**) and Fc[CO-DFLFLA-OMe]<sub>2</sub> (**2b**), respectively. In addition, Fc[CO-LFDFLA-OMe][CO-LFLFLA-OMe] (**2e**), having two nonsymmetrical peptide chains, possess a “Herrick conformation” while a type II β-turn structure only for heterochiral peptide chain. This suggests that fine modulation of helically organized order conformation is possible by selecting an amino acid of proper chirality in disubstituted Fc conjugates.

Overall, the results revealed that control of intra- and/or intermolecular hydrogen bonds is possible in designing these Fc-peptide gels. The architectural control of dimensional structures, utilizing the short amyloid peptide (Aβ19–21) chain possessing chiral centers and hydrogen bonding sites can be considered a useful approach for manipulating the gels, artificial ordered systems and tuning of redox active nanoscale mor-

phologies. Regarding redox responsive properties, the changes in self-assembly and morphologies upon oxidation of all Fc-peptide conjugates are currently under investigation in our laboratory. The introduction of ferrocene to the toolbox of supramolecular gels can significantly expand the possibilities for the manipulation of these smart soft materials with redox responsiveness.

## Experimental Section

### General synthesis of ferrocene bioconjugates

Ferrocenemonocarboxylic acid, 1,1'-ferrocenedicarboxylic acid and 1,1'-ferrocenecarboxylic acid methyl ester were synthesized according to literature procedures.<sup>[69,71]</sup> The synthesis of the other two ferrocene precursors 1,1'-Fc[CO-NHC<sub>10</sub>H<sub>21</sub>][COOH] and Fc[C<sub>3</sub>H<sub>6</sub>-COOH]<sub>2</sub> can be found in the Supporting Information (Scheme S1). The general scheme for the synthesis of Fc-peptide conjugates is given in the Supporting Information (Schemes S2 and S3). All the coupling reactions for Fc-peptide conjugates were carried out using the standard EDC/HOBt method.<sup>[69,71]</sup> The crude product was purified by flash chromatography (SiO<sub>2</sub>, 230–400 mesh) using DCM/MeOH gradient. The *R<sub>f</sub>* values are summarized in the Table S4 in the Supporting Information. All the Fc-peptide conjugates (1–5) were fully characterized by using ESI-TOF mass spectrometry, 1D proton, 1D carbon, 2D COSY and 2D gHMBCAD NMR spectroscopy (see the Supporting Information). Methanol was used as solvent for all ESI-TOF mass spectrometric studies.

### NMR study

Room temperature (22 °C) 1D proton and 2D COSY spectra were recorded on a Bruker Advanced 500 spectrometer (operating at 500 MHz for <sup>1</sup>H and 125 MHz for <sup>13</sup>C). The spectrometer was equipped with a four channel (<sup>1</sup>H, <sup>13</sup>C, <sup>19</sup>F, D) direct broad band observed probe. 2D gHMBCAD spectra were acquired at 50 °C on an Agilent DD2 spectrometer operating at 699.805 MHz for <sup>1</sup>H and 175.981 for <sup>13</sup>C (Agilent, Walnut Creek). The spectrometer was equipped with a 5 mm HFCN cold probe. CDCl<sub>3</sub> and [D<sub>8</sub>]Tol were used as NMR spectroscopy solvents for all Fc conjugates. For characterization of all Fc conjugates, <sup>1</sup>H and <sup>13</sup>C NMR spectroscopy studies were performed at a concentration of 5 and 10 mM, respectively. Variable concentration NMR (VC-NMR) and variable solvent NMR (VS-NMR) spectroscopy studies were carried out on the Bruker Advanced 500 spectrometer at 22 °C.

### Circular dichroism (CD) studies

CD spectroscopy was used to determine the ferrocene conformation and metallocene chirality of Fc-peptide conjugates. CD spectra were recorded in the range 200–600 nm with a JASCO J-810 spectrometer using a 1 mm path-length cell. All CD experiments were carried out in chloroform and toluene at concentrations of 5 mM.

### Crystallographic analysis

Crystallographic data were collected on a Bruker Kappa APEX-DUO diffractometer using a Copper ImuS tube with multilayer optics or monochromated (Triumph) Mo<sub>Kα</sub> radiation which were measured using a combination of  $\varphi$  scans and  $\omega$  scans. The data were processed using APEX2 and SAINT (Bruker, 2007). Absorption corrections were carried out using SADABS (Bruker, 2007). The structures

were solved and refined using SHELXTL (Sheldrick, 2008) for full-matrix least-squares refinement that was based on *F*<sup>2</sup>. All H atoms were included in calculated positions and allowed to refine in riding-motion approximation with U–iso–tied to the carrier atom. CCDC 1052207 and 1052208 contain the supplementary crystallographic data for this paper. These data are provided free of charge by The Cambridge Crystallographic Data Centre.

### Gelation studies

Gel formation was confirmed by the vial-inversion method. Minimum gelation concentration (mgc) of a gel was measured using a glass vial with inner diameter 1.2 cm.

### Transmission electron microscopic (TEM) studies

TEM images were recorded by using a Hitachi 7500 transmission EM. Self-assembled gels/aggregates were dried on formvar-coated copper grids (300 mesh) by slow evaporation in air, then allowed to dry separately in a vacuum. The samples were prepared with gels having their respective mgc concentrations.

### Rheological studies

The Discovery HR2 (TA Instruments) rheometer was used to perform rheological studies with cone-plate geometry in a Peltier plate. The frequency sweep experiments were performed at 0.1% strain.

## Acknowledgements

This work was supported by the NSERC and the University of Toronto Scarborough. We would like to thank Tony Adamo and Darcy Burns for their assistance in data collection.

**Keywords:** chirality · conformational analysis · ferrocene · gels · peptides

- [1] S. S. Babu, V. K. Praveen, A. Ajayaghosh, *Chem. Rev.* **2014**, *114*, 1973.
- [2] G. Yu, X. Yan, C. Han, F. Huang, *Chem. Soc. Rev.* **2013**, *42*, 6697.
- [3] H. Wang, Y. Shi, L. Wang, Z. Yang, *Chem. Soc. Rev.* **2013**, *42*, 891.
- [4] M. D. Segarra-Maset, V. J. Nebot, J. F. Miravet, B. Escuder, *Chem. Soc. Rev.* **2013**, *42*, 7086.
- [5] J. Raeburn, A. Z. Cardoso, D. J. Adams, *Chem. Soc. Rev.* **2013**, *42*, 5143.
- [6] A. Dawn, T. Shiraki, S. Haraguchi, S. Tamaru, S. Shinkai, *Chem. Asian J.* **2011**, *6*, 266.
- [7] M. O. Piepenbrock, G. O. Lloyd, N. Clarke, J. W. Steed, *Chem. Rev.* **2010**, *110*, 1960.
- [8] S. Banerjee, R. K. Das, U. Maitra, *J. Mater. Chem.* **2009**, *19*, 6649.
- [9] A. R. Hirst, B. Escuder, J. F. Miravet, D. K. Smith, *Angew. Chem. Int. Ed.* **2008**, *47*, 8002; *Angew. Chem.* **2008**, *120*, 8122.
- [10] Y. Hisamatsu, S. Banerjee, M. B. Avinash, T. Govindaraju, C. Schmuck, *Angew. Chem. Int. Ed.* **2013**, *52*, 12550; *Angew. Chem.* **2013**, *125*, 12782.
- [11] S. R. Jadhav, P. K. Vemula, R. Kumar, S. R. Raghavan, G. John, *Angew. Chem. Int. Ed.* **2010**, *49*, 7695; *Angew. Chem.* **2010**, *122*, 7861.
- [12] P. W. J. M. Frederix, G. G. Scott, Y. M. Abul-Hajja, D. Kalafatovic, C. G. Pappas, N. Javid, N. T. Hunt, R. V. Ulijn, T. Tuttle, *Nat. Chem.* **2015**, *7*, 30.
- [13] M. Ikeda, T. Tanida, T. Yoshii, K. Kurotani, S. Onogi, K. Urayama, I. Hamachi, *Nat. Chem.* **2014**, *6*, 511.
- [14] G. Fichman, E. Gazit, *Acta Biomater.* **2014**, *10*, 1671.
- [15] H. Cui, A. G. Cheetham, E. T. Pashuck, S. I. Stupp, *J. Am. Chem. Soc.* **2014**, *136*, 12461.
- [16] C. Tomasini, N. Castellucci, *Chem. Soc. Rev.* **2013**, *42*, 156.
- [17] H. Ceylan, M. Urel, T. S. Erkal, A. B. Tekinay, A. Dana, M. O. Guler, *Adv. Funct. Mater.* **2013**, *23*, 2081.

- [18] R. J. Swanekamp, J. T. DiMaio, C. J. Bowerman, B. L. Nilsson, *J. Am. Chem. Soc.* **2012**, *134*, 5556.
- [19] S. Sim, Y. Kim, T. Kim, S. Lim, M. Lee, *J. Am. Chem. Soc.* **2012**, *134*, 20270.
- [20] J. Li, J. M. Carnall, M. C. Stuart, S. Otto, *Angew. Chem. Int. Ed.* **2011**, *50*, 8384; *Angew. Chem.* **2011**, *123*, 8534.
- [21] I. W. Hamley, *Soft Matter* **2011**, *7*, 4122.
- [22] D. J. Adams, P. D. Topham, *Soft Matter* **2010**, *6*, 3707.
- [23] Z. Yang, G. Liang, B. Xu, *Acc. Chem. Res.* **2008**, *41*, 315.
- [24] J. D. Tovar, *Acc. Chem. Res.* **2013**, *46*, 1527.
- [25] H. Frauenrath, E. Jahnke, *Chem. Eur. J.* **2008**, *14*, 2942.
- [26] E.-K. Schillinger, E. Mena-Osteritz, J. Hentschel, H. G. Börner, P. Bäuerle, *Adv. Mater.* **2009**, *21*, 1562.
- [27] B. Adhikari, A. Banerjee, *J. Indian Inst. Sci.* **2012**, *91*, 471.
- [28] J. K. Gallaher, E. J. Aitken, R. A. Keyzers, J. M. Hodgkiss, *Chem. Commun.* **2012**, *48*, 7961.
- [29] U. Lewandowska, W. Zajaczkowski, L. Chen, F. Bouillière, D. Wang, K. Koynov, W. Pisula, K. Müllen, H. Wennemers, *Angew. Chem. Int. Ed.* **2014**, *53*, 12537; *Angew. Chem.* **2014**, *126*, 12745.
- [30] C. Maity, W. E. Hendriksen, J. H. van Esch, R. Eelkema, *Angew. Chem. Int. Ed.* **2015**, *54*, 998; *Angew. Chem.* **2015**, *127*, 1012.
- [31] C. Wang, Q. Chen, F. Sun, D. Zhang, G. Zhang, Y. Huang, R. Zhao, D. Zhu, *J. Am. Chem. Soc.* **2010**, *132*, 3092.
- [32] Z. Qiu, H. Yu, J. Li, Y. Wang, Y. Zhang, *Chem. Commun.* **2009**, 3342.
- [33] J. W. Chung, S. J. Yoon, S. J. Lim, B. K. An, S. Y. Park, *Angew. Chem. Int. Ed.* **2009**, *48*, 7030; *Angew. Chem.* **2009**, *121*, 7164.
- [34] A. Dehsorkhi, V. Castelletto, I. W. Hamley, J. Adamcik, R. Mezzenga, *Soft Matter* **2013**, *9*, 6033.
- [35] C. G. Pappas, T. Mutasa, P. W. J. M. Frederix, S. Fleming, S. Bai, S. Debnath, S. M. Kelly, A. Gachagan, R. V. Ulijn, *Mater. Horiz.* **2015**, *2*, 198–202.
- [36] X. Yu, L. Chen, M. Zhang, T. Yi, *Chem. Soc. Rev.* **2014**, *43*, 5346.
- [37] K. Isozaki, H. Takaya, T. Naota, *Angew. Chem. Int. Ed.* **2007**, *46*, 2855; *Angew. Chem.* **2007**, *119*, 2913.
- [38] Y. Gao, F. Zhao, Q. Wang, Y. Zhang, B. Xu, *Chem. Soc. Rev.* **2010**, *39*, 3425.
- [39] J. W. Sadownik, J. Leckie, R. V. Ulijn, *Chem. Commun.* **2011**, 47, 728.
- [40] Z. Sun, Z. Li, Y. He, R. Shen, L. Deng, M. Yang, Y. Liang, Y. Zhang, *J. Am. Chem. Soc.* **2013**, *135*, 13379.
- [41] R. Ahmed, A. Priimagi, C. F. J. Faul, I. Manners, *Adv. Mater.* **2012**, *24*, 926.
- [42] M. Nakahata, Y. Takashima, H. Yamaguchi, A. Harada, *Nat. Commun.* **2011**, *2*, 511.
- [43] J. Liu, P. He, J. Yan, X. Fang, J. Peng, K. Liu, Y. Fang, *Adv. Mater.* **2008**, *20*, 2508.
- [44] S. Yagai, *Bull. Chem. Soc. Jpn.* **2015**, *88*, 28.
- [45] D. González-Rodríguez, A. P. H. J. Schenning, *Chem. Mater.* **2011**, *23*, 310.
- [46] T. Rehm, C. Schmuck, *Chem. Commun.* **2008**, 801.
- [47] A. T. ten Cate, R. P. Sijbesma, *Macromol. Rapid Commun.* **2002**, *23*, 1094.
- [48] P. Duan, H. Cao, L. Zhang, M. Liu, *Soft Matter* **2014**, *10*, 5428.
- [49] D. K. Smith, *Chem. Soc. Rev.* **2009**, *38*, 684.
- [50] B. Adhikari, J. Nanda, A. Banerjee, *Soft Matter* **2011**, *7*, 8913.
- [51] W. Edwards, D. K. Smith, *J. Am. Chem. Soc.* **2014**, *136*, 1116.
- [52] K. J. Nagy, M. C. Giano, A. Jin, D. J. Pochan, J. P. Schneider, *J. Am. Chem. Soc.* **2011**, *133*, 14975.
- [53] M. B. Taraban, Y. Feng, B. Hammouda, L. L. Hyland, Y. B. Yu, *Chem. Mater.* **2012**, *24*, 2299.
- [54] G.-F. Liu, D. Zhang, C.-L. Feng, *Angew. Chem. Int. Ed.* **2014**, *53*, 7789; *Angew. Chem.* **2014**, *126*, 7923.
- [55] A. Friggeri, C. van der Pol, K. J. C. van Bommel, A. Heeres, M. C. A. Stuart, B. L. Feringa, J. van Esch, *Chem. Eur. J.* **2005**, *11*, 5353.
- [56] A. R. Hirst, D. K. Smith, M. C. Feiters, H. P. M. Geurts, *Chem. Eur. J.* **2004**, *10*, 5901.
- [57] S. Marchesan, C. D. Easton, F. Kushkaki, L. Waddington, P. G. Hartley, *Chem. Commun.* **2012**, *48*, 2195.
- [58] S. Marchesan, C. D. Easton, K. E. Styan, L. J. Waddington, F. Kushkaki, L. Goodall, K. M. McLean, J. S. Forsythe, P. G. Hartley, *Nanoscale* **2014**, *6*, 5172.
- [59] D. Siebler, C. Forster, K. Heinze, *Dalton Trans.* **2011**, *40*, 3558.
- [60] L.-Y. Cheng, Y.-T. Long, H.-B. Kraatz, H. Tian, *Chem. Sci.* **2011**, *2*, 1515.
- [61] S. R. Beeren, J. K. M. Sanders, *Chem. Sci.* **2011**, *2*, 1560.
- [62] T. Moriuchi, T. Hirao, *Acc. Chem. Res.* **2010**, *43*, 1040.
- [63] S. I. Kirin, U. Schatzschneider, S. D. Köster, D. Siebler, N. Metzler-Nolte, *Inorg. Chim. Acta* **2009**, *362*, 894.
- [64] J. Lapić, G. Pavlović, D. Siebler, K. Heinze, V. Rapić, *Organometallics* **2008**, *27*, 726.
- [65] S. Chowdhury, G. Schatte, H. B. Kraatz, *Angew. Chem. Int. Ed.* **2008**, *47*, 7056; *Angew. Chem.* **2008**, *120*, 7164.
- [66] X. de Hatten, Z. Cournia, I. Huc, J. C. Smith, N. Metzler-Nolte, *Chem. Eur. J.* **2007**, *13*, 8139.
- [67] S. I. Kirin, H. B. Kraatz, N. Metzler-Nolte, *Chem. Soc. Rev.* **2006**, *35*, 348.
- [68] D. R. van Staveren, N. Metzler-Nolte, *Chem. Rev.* **2004**, *104*, 5931.
- [69] B. Adhikari, H. B. Kraatz, *Chem. Commun.* **2014**, *50*, 5551.
- [70] R. Afrasiabi, H. B. Kraatz, *Chem. Eur. J.* **2013**, *19*, 17296.
- [71] B. Adhikari, A. J. Lough, B. Barker, A. Shah, C. Xiang, H.-B. Kraatz, *Organometallics* **2014**, *33*, 4873.
- [72] L. Barišić, M. Čakić, K. A. Mahmoud, Y. n. Liu, H. B. Kraatz, H. Pritzkow, S. I. Kirin, N. Metzler-Nolte, V. Rapić, *Chem. Eur. J.* **2006**, *12*, 4965.
- [73] J. Lapić, S. Djaković, M. Cetina, K. Heinze, V. Rapić, *Eur. J. Inorg. Chem.* **2010**, 106.
- [74] E. G. Hutchinson, J. M. Thornton, *Protein Sci.* **1994**, *3*, 2207.
- [75] H. E. Stanger, S. H. Gellman, *J. Am. Chem. Soc.* **1998**, *120*, 4236.
- [76] F. Gao, Y. Li, Y. Sha, L. Lai, Y. Wang, H. Wu, Y. Qiu, *J. Pep. Res.* **2002**, *60*, 75.
- [77] R. Rai, S. Ragothama, R. Sridharan, P. Balam, *Pept. Sci.* **2007**, *88*, 350.
- [78] B. Eckhardt, W. Grosse, L.-O. Essen, A. Geyer, *Proc. Natl. Acad. Sci. USA* **2010**, *107*, 18336.
- [79] P. Jana, S. Maity, S. K. Maity, D. Haldar, *Chem. Commun.* **2011**, *47*, 2092.
- [80] R. Sonti, R. Rai, S. Ragothama, P. Balam, *J. Phys. Chem. B* **2012**, *116*, 14207.
- [81] T. Moriuchi, T. Nagai, T. Hirao, *Org. Lett.* **2006**, *8*, 31.

Received: April 9, 2015

Published online on June 29, 2015